Turbulent-laminar patterns in shear flows without walls

Matthew Chantry[1], Laurette S. Tuckerman[1] and Dwight Barkley[2]

[1]Laboratoire de Physique et Mécanique des Milieux Hétérogènes (PMMH), UMR CNRS 7636; PSL - ESPCI, 10 rue Vauquelin, 75005 Paris, France; Sorbonne Université - UPMC, Univ. Paris 06; Sorbonne Paris Cité - UDD, Univ. Paris 07

[2]Mathematics Institute, University of Warwick, CV4 7AL Coventry, United Kingdom

(Received 18 February 2016)

Turbulent-laminar intermittency, typically in the form of bands and spots, is a ubiquitous feature of the route to turbulence in wall-bounded shear flows. Here we study the idealised shear between stress-free boundaries driven by a sinusoidal body force and demonstrate quantitative agreement between turbulence in this flow and that found in the interior of plane Couette flow – the region excluding the boundary layers. Exploiting the absence of boundary layers, we construct a model flow that uses only four Fourier modes in the shear direction and yet robustly captures the range of spatio-temporal phenomena observed in transition, from spot growth to turbulent bands and uniform turbulence. The model substantially reduces the cost of simulating intermittent turbulent structures while maintaining the essential physics and a direct connection to the Navier-Stokes equations. We demonstrate the generic nature of this process by introducing stress-free equivalent flows for plane Poiseuille and pipe flows which again capture the turbulent-laminar structures seen in transition.

1. Introduction

The onset of turbulence in wall-bounded shear flows is associated with strong intermittency, in which turbulent and laminar flow compete on long spatial and temporal scales. More than a mere curiosity, this intermittency plays a key role in the route to turbulence in many shear flows. Intermittent turbulence is well illustrated by decreasing the Reynolds number in plane Couette flow – the flow between parallel rigid walls moving at different speeds. For sufficiently large Reynolds numbers, the flow is fully turbulent and the fluid volume is uniformly filled with characteristic streamwise streaks and rolls of wall-bounded turbulence [Fig. 1(a)]. With decreasing Reynolds number, intermittency first arises as a large-scale modulation of the turbulent streak-roll structures, eventually resulting in persistent oblique bands of alternating turbulent and laminar flow [Fig. 1(c)]. As the Reynolds number is lowered further, the percentage of turbulent flow decreases until eventually the system returns to fully laminar flow via a percolation transition (Pomeau 1986; Bottin & Chaté 1998; Shi *et al.* 2013; Manneville 2015). In the case of pipe flow, significant progress has been made in understanding the various stages of the transition process (Moxey & Barkley 2010; Avila *et al.* 2011; Barkley 2011; Barkley *et al.* 2015). However, in systems with two extended directions such as plane Couette flow (Prigent *et al.* 2002, 2003; Barkley & Tuckerman 2005; Duguet *et al.* 2010), Taylor-Couette flow (Coles 1965; Meseguer *et al.* 2009; Prigent *et al.* 2002) and plane Poiseuille flow (Tsukahara *et al.* 2014; Tuckerman *et al.* 2014), many basic questions remain concerning the formation and maintenance of turbulent bands and the exact nature of the per-

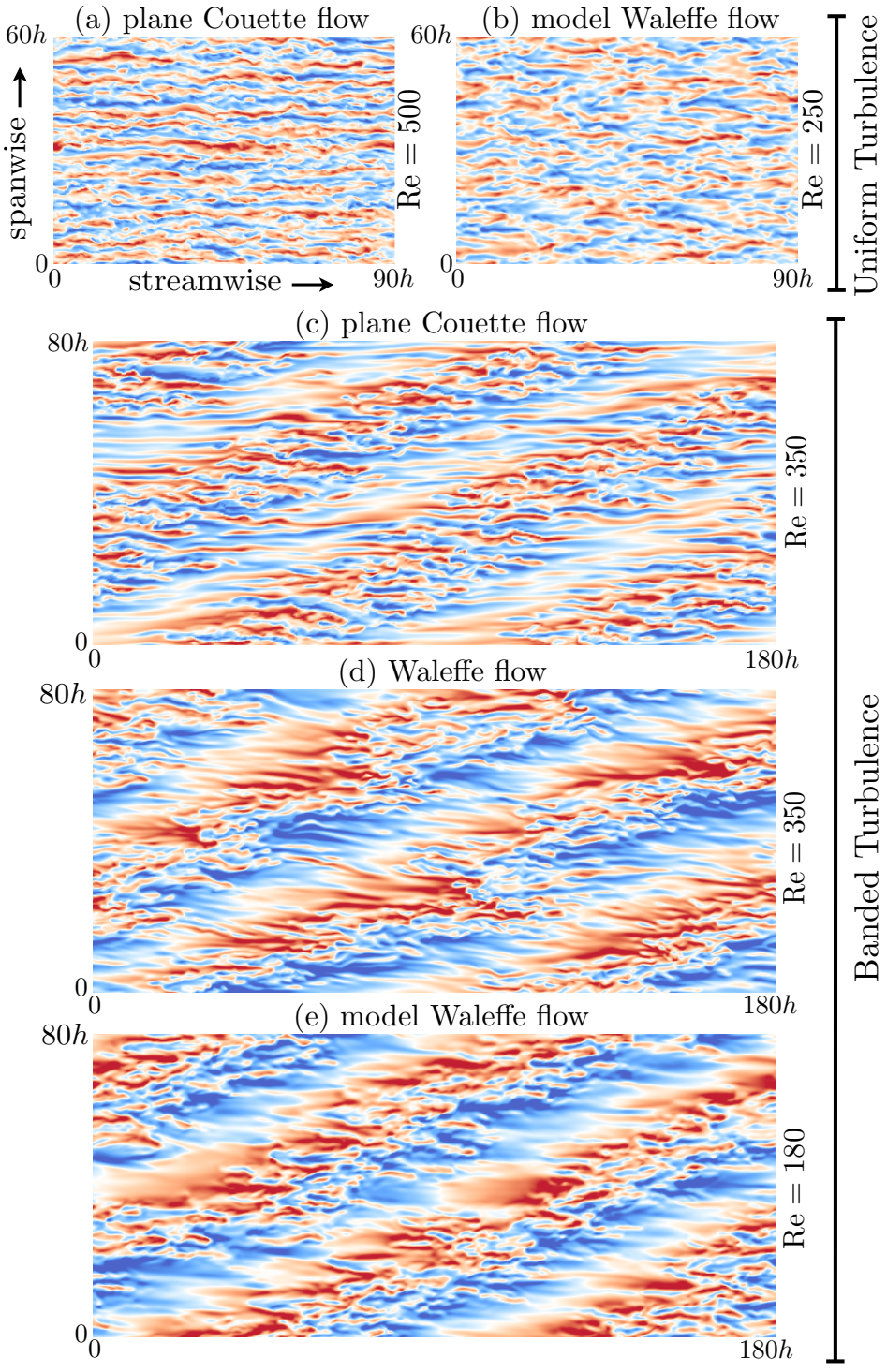

FIGURE 1. Uniform and banded turbulence visualised by instantaneous streamwise velocity at the midplane, with contours from negative (blue) to positive (red) velocity. (a) At high Re, shear turbulence uniformly fills the plane Couette geometry with characteristic low- and high-speed streaks. (b) Comparable uniform turbulence in model Waleffe flow (introduced below). At lower Re, banded turbulence is observed in (c) plane Couette flow, (d) Waleffe flow, and (e) model Waleffe flow.

colation transition, despite efforts to model and understand these features (Manneville 2004, 2009, 2015; Lagha & Manneville 2007*a*,*b*; Barkley & Tuckerman 2007; Duguet & Schlatter 2013; Shi *et al.* 2013; Seshasayanan & Manneville 2015).

Plane Couette flow (PCF) is generally viewed as the ideal system in which to investigate shear turbulence due to its geometric simplicity and the constant shear rate of its laminar flow. In the turbulent regime, however, the mean shear is far from constant. Instead it has a low-shear core and higher-shear boundary layers associated with rigid walls. To this end, we study a flow that surpasses PCF as an ideal computational scenario for transition because the turbulent mean shear is nearly constant at transitional Reynolds numbers. We show that the planar shear flow between stress-free boundaries driven by sinusoidal body forcing reproduces the qualitative phenomena and quantitative profiles of the core region of PCF; it has the dual advantage of requiring far lower spatial resolution for fully resolved simulations and lending itself to faithful model reduction.

In fully turbulent plane Poiseuille flow (PPF), other authors have studied wall-bounded turbulence without walls by modelling the boundary layers combined with POD and LES frameworks (e.g. Podvin & Fraigneau 2011; Mizuno & Jiménez 2013). Here, we will adapt our stress-free approach to study plane Poiseuille and pipe flows at transitional Reynolds numbers.

2. Waleffe flow

Plane Couette flow is generated by rigid parallel walls located at $y = \pm h$ moving with opposite velocities $\pm U$ in the streamwise direction. In contrast, the system we consider is driven by a sinusoidal body force to produce a laminar shear profile confined by stress-free boundary conditions

$$u_{\mathrm{lam}}(y) = V \sin\Big(\frac{\pi}{2}\frac{y}{H}\Big), \qquad v(y=\pm H) = \left.\frac{\partial u}{\partial y}\right|_{\pm H} = \left.\frac{\partial w}{\partial y}\right|_{\pm H} = 0, \tag{2.1}$$

depicted in Fig. 2(a). Typically, periodic boundary conditions are imposed in the lateral streamwise, x, and spanwise, z, directions. The flow was first used by Tollmien to illustrate the insufficiency of an inflection point for linear instability (Drazin & Reid 2004). Its simplicity derives from the stress-free boundary conditions, much as stress-free boundaries have led to simplicity and insight in thermal convection (Drazin & Reid 2004). Waleffe (1997) used the flow to illustrate the self-sustaining process and to derive a model of eight ordinary differential equations (ODEs) capturing the essence of the process. Extensions of this ODE model have been derived (Manneville 2004) and used to measure turbulent lifetimes (Moehlis *et al.* 2004; Dawes & Giles 2011) as well as to find unstable solutions (Moehlis *et al.* 2005; Chantry & Kerswell 2015; Beaume *et al.* 2015). However, there has been little study of fully-resolved Waleffe flow itself in the context of turbulence. Schumacher & Eckhardt (2001) studied the lateral growth of turbulent spots and Doering *et al.* (2003) considered the bounds on energy dissipation in this system. Here, we undertake a systematic study of Waleffe flow throughout the transitional regime.

We simulate Waleffe flow with the freely available `CHANNELFLOW` (Gibson *et al.* 2008; Gibson 2014) adapted to enforce stress-free boundary conditions. We employ 33 Chebyshev modes in the vertical direction, y, and approximately 128 Fourier modes per ten spatial horizontal units.

We begin by comparing turbulent velocity profiles for Waleffe and plane Couette flow, and use these to establish a scaling relationship between the flows. Figure 2 shows the streamwise velocity of uniformly turbulent flow, averaged over time and the horizontal

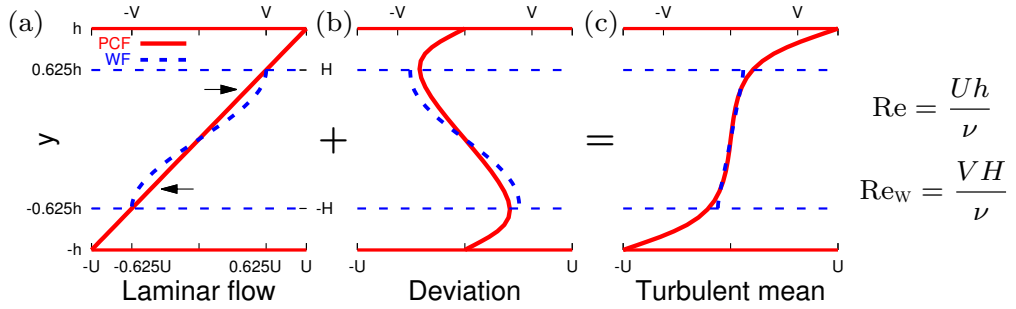

FIGURE 2. Waleffe flow seen as an approximation to the interior of plane Couette flow. Shown are streamwise velocity profiles for PCF (solid/red) and WF (dashed/blue) in the uniformly turbulent regime (PCF: Re = 500 and WF: $\mathrm{Re_W}$ = 500). Plotted are (a) laminar flow, (b) deviation of mean turbulent profile from laminar flow, and (c) mean turbulent profile. The y-scale of WF is non-dimensionalised using $h = 1.6H$ to align its stress-free boundaries (dashed horizontals) with extrema of PCF deviation profile in (b). WF velocities are likewise scaled by $U = 1.6V$ so that both flows have the same average laminar shear in (a). Data are from simulations of 2000 advective time units for $[L_x, L_y, L_z] = [12, 2, 10]h$.

directions, decomposed into the sum of the laminar profile and the deviation from laminar. Lengths in WF have been scaled to align its stress-free boundaries with the extrema of the PCF deviation profile [Fig. 2(b)] and velocities have been scaled to maintain the average laminar shear [Fig. 2(a)]. WF effectively captures the interior section of PCF – the section between the extrema of the deviation profile, Fig. 2(b), or equivalently the section excluding the boundary layers associated with no-slip walls, Fig. 2(c). This was first observed by Waleffe (2003) for an exact solution (exact coherent structure) shared by PCF and by another stress-free version of PCF.

The preceding paragraph implies that when treating WF as the interior of PCF, WF should be non-dimensionalised by length and velocity scales given by $H = h/1.6 = 0.625h$ and $V = 0.625U$. These values are not intended to be exact, since the extrema of the PCF profiles depend on Re, although weakly over the range of interest here (from $y/h \simeq \pm 0.60$ at Re = 300 to $y/h \simeq \pm 0.65$ at Re = 700). This rescaling of y is almost identical to that arrived at by Waleffe (2003) through a different line of reasoning. A value close to this one could also be obtained from the extrema of low-order polynomial approximations, like those used for modelling by Lagha & Manneville (2007*a*,*b*), although these y values would necessarily deviate from the actual values with increasing Reynolds number. The effective Reynolds number for WF, comparable to that for PCF, is then

$$\mathrm{Re} \equiv \frac{Uh}{\nu} = \frac{(1.6V)(1.6H)}{\nu} = 2.56\mathrm{Re_W}. \tag{2.2}$$

where $\mathrm{Re_W} \equiv VH/\nu$ is the Reynolds number usually used for WF.

Simulating Waleffe flow in large domains, we observe robust turbulent bands emerging from uniform turbulence as the Reynolds number is decreased. Figure 1(d) shows such bands under conditions equivalent to those for PCF in Fig. 1(c). There is remarkably strong resemblance in the broad features of the two flows. The primary difference is that in WF, the positive (red) and negative (blue) streaks are less distinct and are almost entirely separated by the turbulent band center, while in PCF the streaks are more sharply defined and may pass through the turbulent center.

For a quantitative study of the banded structure, we simulate the flows in domains tilted by angle θ in the streamwise-spanwise plane as illustrated in Fig. 3(d). Tilted domains are the minimal flow unit to capture bands (Barkley & Tuckerman 2005) and

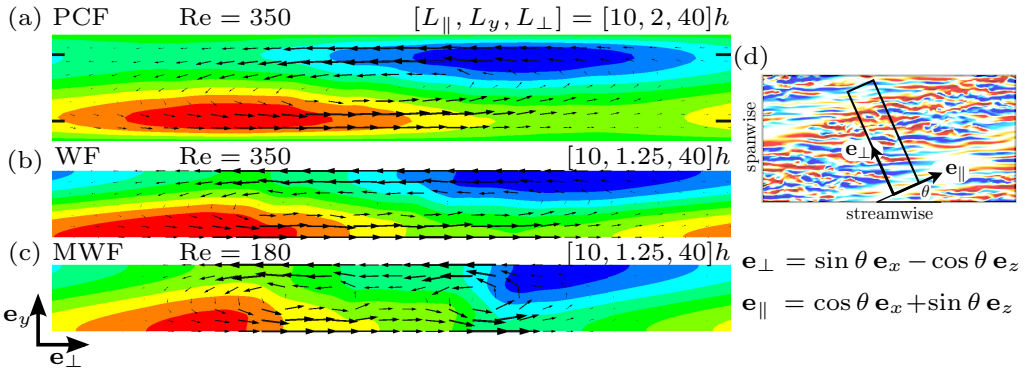

FIGURE 3. Comparison of bands in (a) plane Couette flow, (b) Waleffe flow, and (c) model Waleffe flow, showing the deviation from the laminar flow in a cross-sectional plane, averaged both in t and along $\mathbf{e}_\parallel$. The turbulent region is centered at the middle of the domain. Through-plane flow is depicted by contours from negative (blue) to positive (red) and in-plane flow is depicted by arrows. Contour levels are scaled to 10% below extrema, PCF $\in [-0.34, 0.34]$, WF $\in [-0.42, 0.42]$ and MWF $\in [-0.41, 0.41]$. For visibility the y-direction in all flows has been stretched by a factor of 3. Tic marks at $y = \pm 0.625h$ in frame (a) indicate the bounds of the interior region to which Waleffe flow corresponds. (d) Planar view of a minimal titled domain in relation to a larger domain.

they provide an efficient and focused method for quantitative analysis. Domains are short ($10h - 16h$) in the direction along the bands, $\mathbf{e}_\parallel$, and long ($40h - 120h$) in the direction across the bands, $\mathbf{e}_\perp$, i.e. along the wavevector of the pattern. We fix the angle at $\theta = 24°$, that of the bands seen in Fig. 1. This angle is typical of those observed in experiments and numerical simulations of PCF in large domains (Prigent *et al.* 2002; Duguet *et al.* 2010) and is that used in previous work (Barkley & Tuckerman 2005, 2007; Tuckerman & Barkley 2011) on tilted domains.

In Figs. 3(a) and 3(b) we compare bands in Waleffe flow to those of plane Couette flow, under equivalent conditions using the re-scaling (2.2) of WF. Mean flows are visualised in the $(\mathbf{e}_\perp, \mathbf{e}_y)$-plane, with averages taken over the $\mathbf{e}_\parallel$ direction and over 2000 advective time units. The red and blue regions indicate the flow parallel to the turbulent bands, primarily along the edges of the bands, while the arrows show circulation surrounding them. The banded structure in Waleffe flow is almost identical to that found in the interior of plane Couette flow. Waleffe (2003) made similar observations regarding exact coherent structures in no-slip and stress-free versions of plane Couette flow. The main qualitative difference between the flows is the greater separation of the regions of positive and negative band-aligned flow in WF [Fig. 3(b)]. This is a manifestation of the streak separation in Fig. 1(d).

We also consider the fluctuations, $\tilde{\mathbf{u}}$, about the mean flow. In figure 4 we see that in both PCF and WF the turbulent kinetic energy is largest in the interior. Beneath this we plot $\partial_y \langle \tilde{u}\tilde{v} \rangle$, which dominates the turbulent force. (See Barkley & Tuckerman (2007) for a full discussion of the force balance that prevails in turbulent-laminar banded flow.) Although the turbulent force is very large in the near-wall regions of PCF, it mainly acts to counterbalance the large dissipation due to the steep gradients near the walls. In the interior of PCF, both dissipative and turbulent forces are much weaker, as is the case for the entirety of Waleffe flow.

We have surveyed the intermittency in Waleffe flow as a function of Reynolds number. In the tilted domain, bands emerge from turbulence at Re ≈ 640 and turbulent patches are still observed with long lifetimes ($O(10^3)$ time units) at Re ≈ 250, consistent with

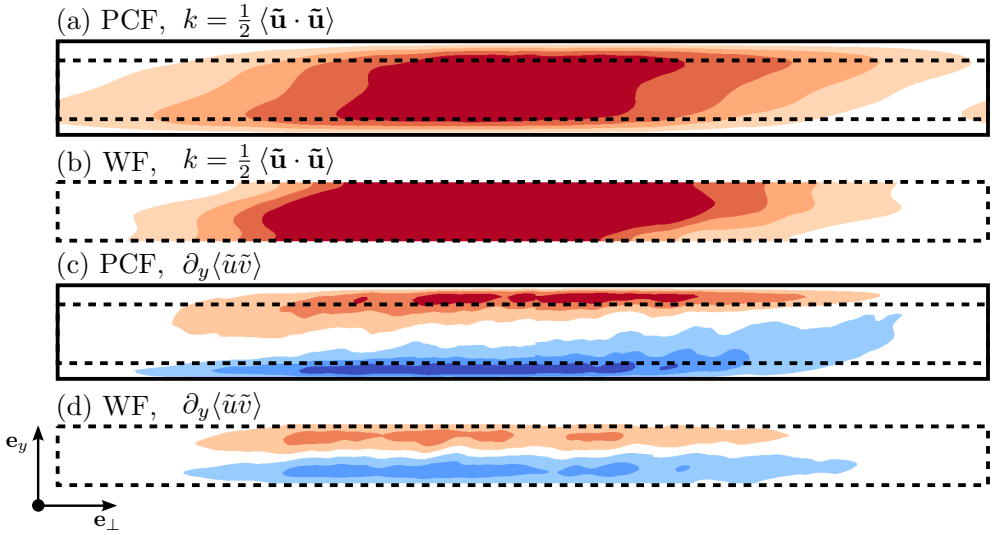

FIGURE 4. Comparison of turbulent fluctuations, $\tilde{\mathbf{u}}$, in plane Couette flow and Waleffe flow for turbulent bands plotted in figure 3. (a,b) Turbulent kinetic energy, $k = \frac{1}{2}\langle \tilde{\mathbf{u}} \cdot \tilde{\mathbf{u}} \rangle$ for PCF, (contours $[0, 0.08]$) and WF (contours $[0, 0.05]$) respectively, averaged as in figure 3(a-c). (c,d) Dominant turbulent force contribution in the band-aligned direction, $\partial_y \langle \tilde{u}\tilde{v} \rangle$ for PCF (contours $[-0.017, 0.017]$) and WF (contours $[-0.017, 0.017]$). Dashed lines in figures (a,c) show the bounds of the interior region to which Waleffe flow corresponds.

$\mathrm{Re_W} = \mathrm{Re}/2.56 \approx 110$ previously found (Schumacher & Eckhardt 2001, Fig. 2). In PCF the equivalent range is $325 \lesssim \mathrm{Re} \lesssim 420$ (Bottin *et al.* 1998; Bottin & Chaté 1998; Shi *et al.* 2013; Tuckerman & Barkley 2011).

3. Modelling Waleffe flow

Motivated by the simplicity of Waleffe flow and its ability to capture turbulent-band formation without the boundary layers present near rigid walls, we have developed a minimal model using only leading Fourier wavenumbers in the shear direction y. Our model of Waleffe flow (MWF) can be written as

$$u(x,y,z) = u_0(x,z) + u_1(x,z)\sin(\beta y) + u_2(x,z)\cos(2\beta y) + u_3(x,z)\sin(3\beta y), \tag{3.1a}$$

$$v(x,y,z) = v_1(x,z)\cos(\beta y) + v_2(x,z)\sin(2\beta y) + v_3(x,z)\cos(3\beta y), \tag{3.1b}$$

$$w(x,y,z) = w_0(x,z) + w_1(x,z)\sin(\beta y) + w_2(x,z)\cos(2\beta y) + w_3(x,z)\sin(3\beta y), \tag{3.1c}$$

where $\beta = \pi/2H$. To further simplify, we use a poloidal-toroidal plus mean-mode representation

$$\mathbf{u} = \nabla \times \psi(x,y,z)\mathbf{e_y} + \nabla \times \nabla \times \phi(x,y,z)\mathbf{e_y} + f(y)\mathbf{e}_x + g(y)\mathbf{e}_z, \tag{3.2}$$

where ψ, f and g match the y-decomposition of u and ϕ that of v. Substituting (3.2) into the Navier-Stokes equations and applying Fourier orthogonality in y, we derive our governing equations, which are seven partial differential equations in (x, z, t) and six ODEs for the mean flows f and g. The original eight-ODE model, derived by Waleffe (1997) to illustrate the self-sustaining process, is contained within the system and can be recovered by reducing the number of modes in y and imposing a single Fourier wavenumber in x and

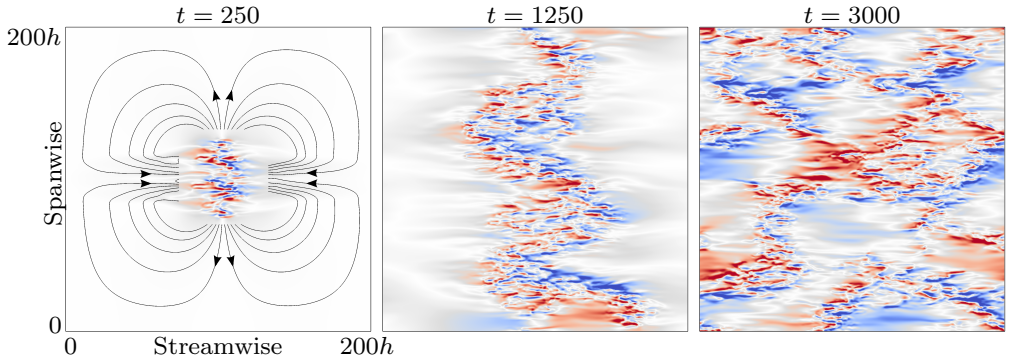

FIGURE 5. Growth of a turbulent spot in model Waleffe flow at Re = 160. The flow is initialised with a poloidal vortex and subsequent evolution is visualised by streamwise velocity at the midplane. At early times ($t = 250$), a large-scale quadrupolar flow dominates as shown by streamlines of the y-averaged flow (contour lines, only plotted away from the spot for visibility). By $t = 1250$ bands begin to develop and form a zigzag across the domain. The bands continue to grow, and by $t = 3000$ a complex array of bands fills the domain.

z. Our model is closely related to a series of models by Manneville and co-workers of WF and PCF (Manneville 2004; Lagha & Manneville 2007*a*,*b*; Seshasayanan & Manneville 2015). The first three of these attempted to capture localised dynamics with only two modes in y. Turbulent bands were not spontaneously formed or maintained; instead, spots grew to uniform turbulence. Most recently, and in parallel with our work, Seshasayanan & Manneville (2015) showed that a model of PCF with four polynomial modes in the wall-normal direction produced oblique bands, albeit over a narrow range of Re.

We simulate the model using a Fourier pseudo-spectral method in (x, z) and time step using backward Euler for the linear terms and Adams-Bashforth for the nonlinear terms. The effective low resolution in y results in a decreased resolution requirement in (x, z), with only four modes needed per spatial unit, compared with ~ 10 for PCF and WF.

At high Re, uniform turbulence is observed in the model [Fig. 1(b)], displaying the usual streamwise-aligned streaks generated by rolls. Streaks in MWF, as well as in WF (not shown), typically have shorter streamwise extent than those in PCF. Reducing Re, bands are found [Fig. 1(e)] which are difficult to distinguish from those in fully resolved Waleffe flow [Fig. 1(d)]; this is also true for bands computed in the tilted domain [Fig. 3(b) and (c)]. The most notable qualitative difference between MWF and WF is the increased separation of the band-aligned flow regions and of the related circulating in-plane flow. We find bands in the model for Reynolds numbers $\mathrm{Re} \in [125, 230]$, a large relative range of Re and an approximate rescaling of $\mathrm{Re} \in [250, 640]$ for fully resolved Waleffe flow. The most likely reason for the shift in Re is the lack of high-curvature modes in the wall-normal direction, i.e. small spatial scales which would be associated with higher dissipation. However, in a model for pipe flow (Willis & Kerswell 2009) with few azimuthal modes, the Re for transition increased relative to that of fully resolved flow.

We investigate the formation of bands via spot growth in the model. As in Schumacher & Eckhardt (2001), laminar flow is seeded with a Gaussian poloidal vortex

$$\mathbf{u} = \nabla \times \nabla \times A \exp\left[-a_x^2 x^2 - a_y^2 y^2 - a_z^2 z^2\right] \mathbf{e}_y, \tag{3.3}$$

here with coefficients $a_x = a_z = 0.25/h$, $a_y = 2/h$. Dependence on y is approximated by projecting onto the four y modes of (3.1). The developing spot in Fig. 5 matches the many facets of spot growth seen in a variety of other shear flows. At early times ($t = 250$), growth is predominantly in the spanwise direction, as has been commonly

observed (Schumacher & Eckhardt 2001; Duguet & Schlatter 2013; Couliou & Monchaux 2015). An accompanying large-scale quadrupolar flow quickly develops, which we indicate in Fig. 5(a) by means of streamlines of the y-averaged flow away from the spot. Quadrupolar flows have been reported around growing spots in PCF (Duguet & Schlatter 2013; Couliou & Monchaux 2015), in Poiseuille flow (Lemoult *et al.* 2014),and in a low-order model for PCF (Lagha & Manneville 2007*a*). At later times, structures develop that are recognisable as oblique bands [compare our $t = 1250$ with Fig. 1 of Duguet & Schlatter (2013)]. By $t = 3000$, these structures have pervaded the whole domain.

4. Plane Poiseuille flow

To further demonstrate the applications of this stress-free modelling we consider plane Poiseuille flow (PPF), generated here by enforcing constant mass flux in the horizontal directions. The laminar profile in a reference frame moving with the mean velocity is shown as the red curve of figure 6(a). A natural extension of the PCF case would be to approximate the parabolic PPF with a cosine body forcing and stress-free boundaries. However, such a flow develops a linear instability at $\mathrm{Re} = 80$, far below expected transition. The bifurcating eigenvector is the stress-free equivalent of the classic Tollmien-Schlichting wave of PPF, which becomes unstable at $\mathrm{Re} = 5772$. To remove this unstable mode, we enforce symmetry across the channel midplane, effectively juxtaposing WF (blue) with its mirror-symmetric counterpart (grey). Because of this, no new simulations are necessary, since all results concerning WF can be used, merely by using the rescaling appropriate to PPF. WF should now be non-dimensionalised by length and velocity scales given by $H = 0.825h/2$ and $V = 0.825^2U/2$. The conventional PPF Reynolds number and the corresponding one for WF in this context are

$$\mathrm{Re} \equiv \frac{Uh}{\nu} = \frac{(2V)(2H)}{0.825^3\nu} \approx 7.12\frac{VH}{\nu} = 7.12\,\mathrm{Re}_\mathrm{w}, \tag{4.1}$$

where U is based on the mean Poiseuille flow. As was the case for PCF these values are not intended to be exact, since the extrema of the PPF profiles depend on Re (from $y/h \simeq \pm 0.78$ at $\mathrm{Re} = 1300$ to $y/h \simeq \pm 0.86$ at $\mathrm{Re} = 2400$). A "true" rescaling of the flow would be Reynolds number dependent but a fixed value suffices for our purpose. As in the PCF case, the length scale found by Waleffe (2003) using the exact coherent structures is close to that found here using the turbulent mean profile; a value within this range could also be obtained from the extrema of the low-order polynomials used by Lagha (2007) to model PPF. Our remapped existence range for bands in Waleffe flow is $\mathrm{Re} \in [700, 1800]$ and compares well with $\mathrm{Re} \in [800, 1900]$ in PPF (Tuckerman *et al.* 2014).

Figure 7 shows the mean structure of turbulent bands in PPF and in its stress-free counterpart. Excluding the boundary layers of PPF, there is very good agreement between the structures in these flows. By construction, the lower half of figure 7(b) is identical to figure 3(b). The lower half of figure 7(a) also strongly resembles 3(a). The resemblance between turbulent bands in these two flows solidifies the prevalent view of PPF as two PCFs (Waleffe 2003; Tuckerman *et al.* 2014).

The low-order model of Waleffe flow derived for PCF in section 3 carries over in a straightforward manner to PPF and is therefore not shown. A five-mode model of wall-bounded PPF was derived by Lagha (2007) and used to study spot growth.

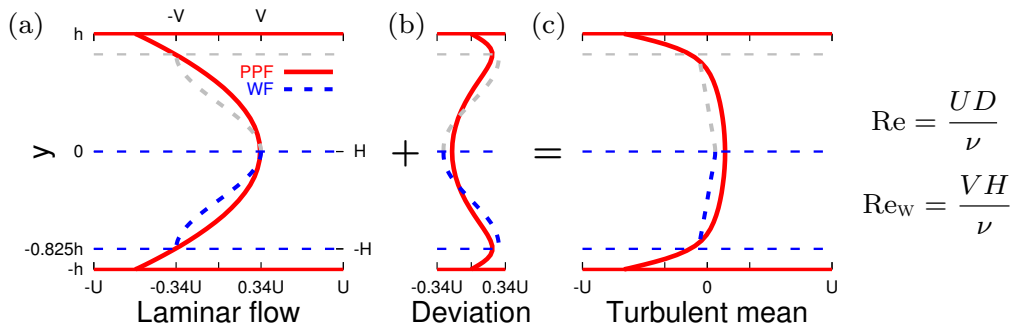

FIGURE 6. Doubled Waleffe flow seen as an approximation to the interior of plane Poiseuille flow. Shown are streamwise velocity profiles for PPF (solid/red) and WF (dashed/blue and grey) in the uniformly turbulent regime (PPF: $\mathrm{Re} = 1800$ and WF: $\mathrm{Re}_\mathrm{w} = 500$). Plotted are (a) laminar flow, (b) deviation of mean turbulent profile from laminar flow, and (c) mean turbulent profile. The y-scale of WF is non-dimensionalised using $H = 2h/0.825$ to align its stress-free boundaries (dashed horizontals) with extrema of PCF deviation profile in (b). WF velocities are likewise scaled by $V = 2U/0.825^2$ so that both flows have same average laminar shear in (a). Data are from simulations of 2000 advective time units for $[L_x, L_y, L_z] = [12, 2, 10]h$.

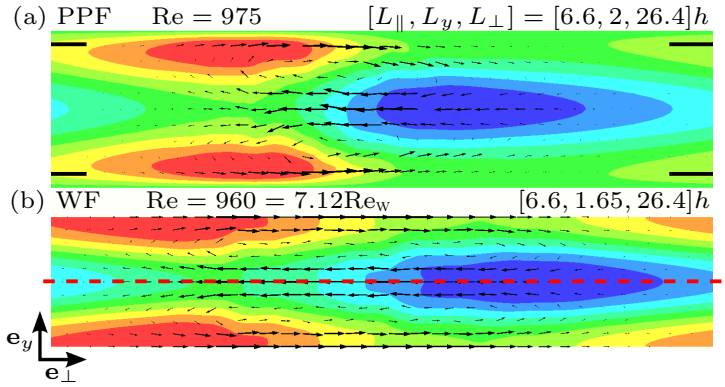

FIGURE 7. Comparison of bands between plane Poiseuille flow (top) and doubled Waleffe flow (bottom). Contours of streamwise velocity $[-0.4, 0.4]$, and arrows for inplane velocity. Domain size and Reynolds number for PPF was chosen to match with the (rescaled) WF bands plotted in figure 3(b). This comparison excels near the midplane in PPF and confirms that PPF can be viewed as two plane Couette flows; compare figures 7(a) and 3(a).

5. Stress-free pipe flow

Finally, we turn to pipe flow (PF), the third canonical wall-bounded shear flow, in which intermittency takes the form of puffs. We introduce a Bessel function body force which drives a laminar flow confined by cylindrical stress-free boundaries

$$u_{z,\mathrm{lam}}(r) = \frac{V}{1 - J_0(k_0')} J_0\left(k_0' \frac{r}{R}\right), \qquad u_r(r = R) = \left.\frac{\partial u_z}{\partial r}\right|_R = \left.\frac{\partial}{\partial r}\left(\frac{u_\theta}{r}\right)\right|_R = 0 \tag{5.1}$$

where $k_0' \approx 3.83$ is the first non-zero root of J_0'.

Simulations are conducted using `openpipeflow.org` (Willis & Kerswell 2009) adapted to enforce stress-free conditions on the pipe walls. As before, we first consider uniform turbulence (figure 8) and nondimensionalise our stress-free flow to match the turning points in the deviation. This results in $R = 0.86\, D/2$ and $V = 0.86^2 \cdot 2U$ and a Reynolds

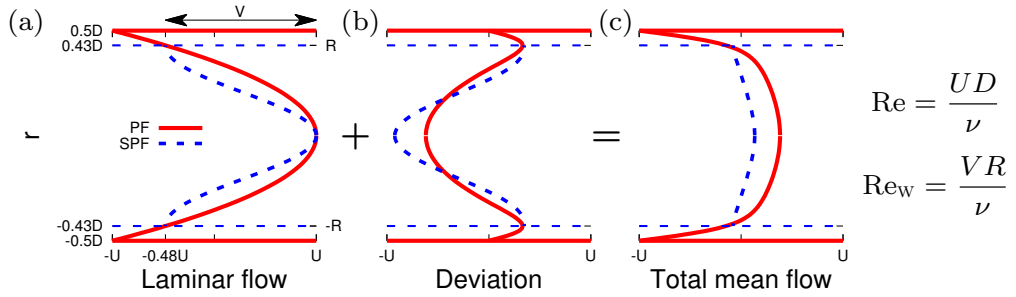

FIGURE 8. Stress-free pipe flow (SPF) seen as an approximation to the interior of pipe flow (PF). Shown are streamwise velocity profiles for PF (solid/red) and SPF (dashed/blue) in the uniformly turbulent regime (PF: Re = 3000 and SPF: $\mathrm{Re_W} = 1900$). Plotted are (a) laminar flow, (b) deviation of mean turbulent profile from laminar flow, and (c) mean turbulent profile. The r-scale of SPF is non-dimensionalised using $R = 0.86D/2$ to align its stress-free boundaries (dashed horizontals) with extrema of PF deviation profile in (b). SPF velocities are likewise scaled by $V = 2 \cdot 0.86^2 U$ so that both flows in (a) have the same average laminar shear. Data are from simulations of 2000 advective time units for pipes of length $5D$.

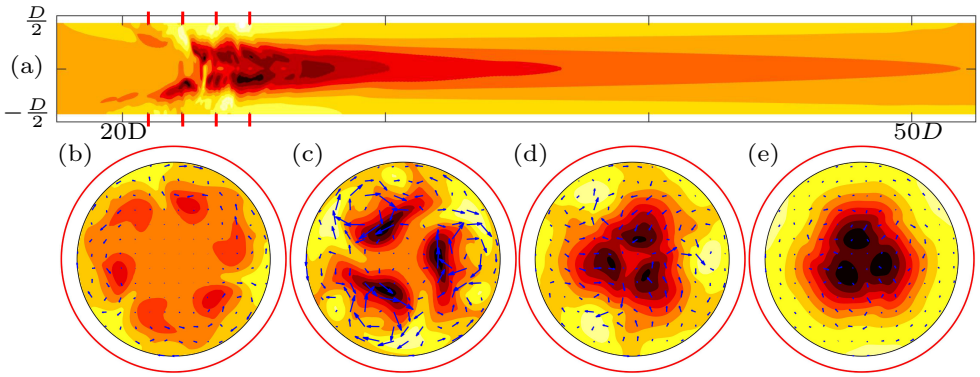

FIGURE 9. A turbulent puff in stress-free pipe flow. (a) Streamwise velocity along the pipe (only partial pipe shown) and (b-e) (r, θ)-slices along the pipe [indicated by red lines in (a)] with arrows of in-plane velocity. Motivated by figure 8 the red circles show the location of the walls for the corresponding wall-bounded flow, highlighting the absence of boundary layers in the stress-free case. Nine contours are used for streamwise velocity varying in [-0.86,0.48].

number

$$\mathrm{Re} = \frac{UD}{\nu} = \frac{VR}{0.86^3\nu} \approx 1.57\mathrm{Re_W}. \tag{5.2}$$

where $D/2$ is the pipe radius and $2U$ is the maximum laminar speed. Like the cosine forced version of PPF, stress-free pipe flow undergoes a linear instability at low Reynolds number ($\mathrm{Re} \approx 340$), below the existence range of turbulence. Therefore to study laminar-turbulent intermittency (here turbulent puffs) we impose the symmetry

$$\mathbf{R}_n : \mathbf{u}(r, \theta, z) \to \mathbf{u}(r, \theta + \tfrac{2\pi}{n}, z), \quad n \geq 2 \tag{5.3}$$

which stabilises the laminar flow. We will only present results from $\mathbf{R}_3$ here but alternative choices (e.g. two and four) produce comparable results.

In this symmetry subspace, turbulent puffs are found for stress-free pipe flow over a range of Reynolds numbers $\mathrm{Re} \in [2400, 3500]$; an exemplar is plotted in figure 9. For conventional rigid-wall pipe flow in this subspace, turbulent puffs are first observed at

Re $\approx$ 2400, an increase from Re $\approx$ 1750 (Darbyshire & Mullin 1995) for no imposed symmetry. The structure and length scales of these puffs are comparable with their wall-bounded counterparts. Excitation occurs upstream, [figure 9(b-c)] generating fast and slow streaks which slowly decay downstream [9(e)]. The success of model Waleffe flow combined with the low-azimuthal-resolution model of Willis & Kerswell (2009) suggests that a model with one spatial dimension (z) is possible. However, the complexity of cylindrical coordinates, particularly the coupled boundary conditions, prevents further work at this time.

6. Conclusion

Since at least the 1960s (e.g. Coles 1962) there has been interest in understanding the ubiquitous turbulent-laminar intermittency observed at the onset of turbulence in wall-bounded shear flows. We have demonstrated that shear alone is the necessary ingredient for generating these structures; the boundary layers of wall-bounded flows are not essential. The robustness of this concept is demonstrated, not only by turbulent bands in stress-free versions of PCF and PPF, but also by puffs in stress-free pipe flow. Our rescaling yields quantitative correspondence to the range of existence and the length scales of these phenomena. In planar geometry, we exploit the absence of rigid walls to propose a simple four-vertical-mode model that captures all the essential physics in the shear-dependent direction. This provides a direct link between ODE models of the self-sustaining process (Waleffe 1997) and the modelling of turbulent-laminar coexistence. The absence of rigid walls opens the possibility of exploring large-scale features of transitional turbulence without the complications and numerical requirements of sharp gradients. This should greatly facilitate the numerical study of percolation in systems with two extended directions, while maintaining a direct connection with the Navier-Stokes equation.

MC was supported by a grant, TRANSFLOW, provided by the Agence Nationale de la Recherche (ANR). This work was performed using high performance computing resources provided by the Institut du Developpement et des Ressources en Informatique Scientifique (IDRIS) of the Centre National de la Recherche Scientifique (CNRS), coordinated by GENCI (Grand Équipement National de Calcul Intensif).

REFERENCES

Avila, K., Moxey, D., de Lozar, A., Avila, M., Barkley, D. & Hof, B. 2011 The onset of turbulence in pipe flow. *Science* **333**, 192–196.

Barkley, D. 2011 Simplifying the complexity of pipe flow. *Phys. Rev. E* **84**, 016309.

Barkley, D., Song, B., Mukund, V., Lemoult, G., Avila, M. & Hof, B. 2015 The rise of fully turbulent flow. *Nature* **526**, 550–553.

Barkley, D. & Tuckerman, L. S. 2005 Computational study of turbulent laminar patterns in Couette flow. *Phys. Rev. Lett.* **94**, 014502.

Barkley, D. & Tuckerman, L. S. 2007 Mean flow of turbulent–laminar patterns in plane Couette flow. *J. Fluid Mech.* **576**, 109–137.

Beaume, C., Chini, G. P., Julien, K. & Knobloch, E. 2015 Reduced description of exact coherent states in parallel shear flows. *Phys. Rev. E* **91**, 043010.

Bottin, S. & Chaté, H. 1998 Statistical analysis of the transition to turbulence in plane Couette flow. *Eur. Phys. J. B* **6**, 143–155.

Bottin, S., Daviaud, F., Manneville, P. & Dauchot, O. 1998 Discontinuous transition to spatiotemporal intermittency in plane Couette flow. *Europhys. Lett.* **43**, 171–176.

Chantry, M. & Kerswell, R. R. 2015 Localization in a spanwise-extended model of plane Couette flow. *Phys. Rev. E* **91**, 043005.

Coles, D. 1962 Interfaces and intermittency in turbulent shear flow. *Mécanique de la Turbulence* **108**, 229–248.

Coles, D. 1965 Transition in circular Couette flow. *J. Fluid Mech.* **21**, 385–425.

Couliou, M. & Monchaux, R. 2015 Large-scale flows in transitional plane Couette flow: A key ingredient of the spot growth mechanism. *Phys. Fluids* **27**, 034101.

Darbyshire, A. G. & Mullin, T. 1995 Transition to turbulence in constant-mass-flux pipe flow. *J. Fluid Mech.* **289**, 83–114.

Dawes, J. H. P. & Giles, W. J. 2011 Turbulent transition in a truncated one-dimensional model for shear flow. *Proc. R. Soc. A* **467**, 3066–3087.

Doering, C. R., Eckhardt, B. & Schumacher, J. 2003 Energy dissipation in body-forced plane shear flow. *J. Fluid Mech.* **494**, 275–284.

Drazin, P. G. & Reid, W. H. 2004 *Hydrodynamic Stability*. Cambridge University Press.

Duguet, Y. & Schlatter, P. 2013 Oblique laminar-turbulent interfaces in plane shear flows. *Phys. Rev. Lett.* **110**, 034502.

Duguet, Y., Schlatter, P. & Henningson, D. S. 2010 Formation of turbulent patterns near the onset of transition in plane Couette flow. *J. Fluid Mech.* **650**, 119–129.

Gibson, J. F. 2014 Channelflow: A spectral Navier-Stokes simulator in C++. *Tech. Rep.*. U. New Hampshire, `Channelflow.org`.

Gibson, J. F., Halcrow, J. & Cvitanović, P. 2008 Visualizing the geometry of state space in plane Couette flow. *J. Fluid Mech.* **611**, 107–130.

Lagha, M. 2007 Turbulent spots and waves in a model for plane poiseuille flow. *Phys. Fluids* **19**, 124103.

Lagha, M. & Manneville, P. 2007*a* Modeling of plane Couette flow. i. large scale flow around turbulent spots. *Phys. Fluids* **19**, 094105.

Lagha, M. & Manneville, P. 2007*b* Modeling transitional plane Couette flow. *Eur. Phys. J. B* **58**, 433–447.

Lemoult, G., Gumowski, K., Aider, J.-L. & Wesfreid, J. E. 2014 Turbulent spots in channel flow: An experimental study. *Eur. Phys. J. E* **37**, 1–11.

Manneville, P. 2004 Spots and turbulent domains in a model of transitional plane Couette flow. *Theor. Comput. Fluid Dyn.* **18**, 169–181.

Manneville, P. 2009 Spatiotemporal perspective on the decay of turbulence in wall-bounded flows. *Phys. Rev. E* **79**, 025301.

Manneville, P. 2015 On the transition to turbulence of wall-bounded flows in general, and plane Couette flow in particular. *Eur. J. Mech. B-Fluid* **49**, 345–362.

Meseguer, A., Mellibovsky, F., Avila, M. & Marques, F. 2009 Instability mechanisms and transition scenarios of spiral turbulence in Taylor-Couette flow. *Phys. Rev. E* **80**, 046315.

Mizuno, Y. & Jiménez, J. 2013 Wall turbulence without walls. *J. Fluid Mech.* **723**, 429–455.

Moehlis, J., Faisst, H. & Eckhardt, B. 2004 A low-dimensional model for turbulent shear flows. *New J. Phys.* **6**, 56.

Moehlis, J., Faisst, H. & Eckhardt, B. 2005 Periodic orbits and chaotic sets in a low-dimensional model for shear flows. *SIAM J. Appl. Dyn. Sys.* **4**, 352–376.

Moxey, D. & Barkley, D. 2010 Distinct large-scale turbulent-laminar states in transitional pipe flow. *Proc. Natl. Acad. Sci. U.S.A.* **107**, 8091–8096.

Podvin, B. & Fraigneau, Y. 2011 Synthetic wall boundary conditions for the direct numerical simulation of wall-bounded turbulence. *J. Turbul.* **12**, 1–26.

Pomeau, Y. 1986 Front motion, metastability and subcritical bifurcations in hydrodynamics. *Physica D* **23**, 3–11.

Prigent, A., Grégoire, G., Chaté, H. & Dauchot, O. 2003 Long-wavelength modulation of turbulent shear flows. *Physica D* **174**, 100–113.

Prigent, A., Grégoire, G., Chaté, H., Dauchot, O. & van Saarloos, W. 2002 Large-scale finite-wavelength modulation within turbulent shear flows. *Phys. Rev. Lett.* **89**, 014501.

Schumacher, J. & Eckhardt, B. 2001 Evolution of turbulent spots in a parallel shear flow. *Phys. Rev. E* **63**, 046307.

Seshasayanan, K. & Manneville, P. 2015 Laminar-turbulent patterning in wall-bounded shear flows: a Galerkin model. *Fluid Dyn. Res.* **47**.

Shi, L., Avila, M. & Hof, B. 2013 Scale invariance at the onset of turbulence in Couette flow. *Phys. Rev. Lett.* **110**, 204502.

Tsukahara, T., Iwamoto, K., Kawamura, H. & Takeda, T. 2014 DNS of heat transfer in transitional channel flow accompanied by turbulent puff-like structure. *arXiv:1406.0586* .

Tuckerman, L. S. & Barkley, D. 2011 Patterns and dynamics in transitional plane Couette flow. *Phys. Fluids* **23**, 041301.

Tuckerman, L. S., Kreilos, T., Schrobsdorff, H., Schneider, T. M. & Gibson, J. F. 2014 Turbulent-laminar patterns in plane Poiseuille flow. *Phys. Fluids* **26**, 114103.

Waleffe, F. 1997 On a self-sustaining process in shear flows. *Phys. Fluids* **9**, 883–900.

Waleffe, F. 2003 Homotopy of exact coherent structures in plane shear flows. *Phys. Fluids* **15**, 1517–1534.

Willis, A. P. & Kerswell, R. R. 2009 Turbulent dynamics of pipe flow captured in a reduced model: puff relaminarization and localized "edge" states. *J. Fluid Mech.* **619**, 213–233.